Article

Not peer-reviewed version

Image quality and quantitative PET parameters of low-dose [18F]FDG PET in a Total-Body PET/CT scanner.

Eduardo Calderón , Fabian P. Schmidt , Wenhong Lan , Salvador Castaneda-Vega , Andreas S. Brendlin , Nils F. Trautwein , Helmut Dittmann , Christian La Fougère , Lena Sophie Kiefer *

Posted Date: 4 October 2023

doi: 10.20944/preprints202310.0113.v1

Keywords: Keywords: Total-Body PET/CT Scanner, LAFOV PET/CT, low-dose [18F]FDG PET, [18F]FDG

Article

Image Quality and Quantitative PET Parameters of Low-Dose [^{18}F]FDG PET in a Total-Body PET/CT Scanner

Eduardo Calderón [1], Fabian P. Schmidt [1,2], Wenhong Lan [1], Salvador Castaneda-Vega [1,2], Andreas S. Brendlin [3], Nils F. Trautwein [1], Helmut Dittmann [1], Christian la Fougère [1,4,5] and Lena Sophie Kiefer [1]*

[1] Department of Nuclear Medicine and Clinical Molecular Imaging, University Hospital Tuebingen, Tuebingen, Germany
[2] Werner Siemens Imaging Center, Department of Preclinical Imaging and Radiopharmacy, Eberhard-Karls University Tuebingen, Tuebingen, Germany
[3] Department of Diagnostic and Interventional Radiology, University Hospital Tuebingen, Tuebingen, Germany
[4] Cluster of Excellence iFIT (EXC 2180) "Image Guided and Functionally Instructed Tumor Therapies", University of Tuebingen, Tuebingen
[5] German Cancer Consortium (DKTK), Partner Site Tuebingen, Germany
* Correspondence: Lena S. Kiefer, lena.kiefer@med.uni-tuebingen.de

Abstract: Total-body PET/CT scanners provide increased sensitivity, enabling the adjustment of imaging parameters by reducing injected activity or shortening acquisition time. This study aimed to evaluate the limitations of reduced [^{18}F]FDG activity doses on image quality, lesion detectability, and quantification of lesion uptake in the Biograph Vision Quadra, as well as to assess the benefits of the recently introduced ultra-high sensitivity mode in a clinical setting. A number of 26 patients who underwent [^{18}F]FDG-PET/CT (3.0 MBq/kg, 5 min. scan time) were included in this analysis. PET raw data was rebinned for shorter frame durations to simulate 5 min. scans with lower activities in high sensitivity (HS) and ultra-high sensitivity (UHS) modes. Image quality, noise, and lesion detectability (n=82) were assessed using a 5-point Likert scale. The coefficient of variation (CoV), signal-to-noise ratio (SNR), tumor-to-background ratio (TBR), and standardized uptake values (SUV) including SUV_{mean}, SUV_{max}, and SUV_{peak} were evaluated. Subjective image ratings were generally superior in UHS compared to HS mode. At 0.5 MBq/kg, lesion detectability decreased to 95% (HS) and 98% (UHS). SNR was comparable at 1.0 MBq/kg in HS (5.7±0.6) and 0.5 MBq/kg in UHS (5.5±0.5). With lower doses, there were negligible reductions in SUV_{mean} and SUV_{peak}, whereas SUV_{max} increased steadily. Reducing [^{18}F]FDG activity to 1.0 MBq/kg (HS/UHS) in a total-body PET/CT provides diagnostic image quality without statistically significant changes in uptake parameters. UHS mode improves image quality, noise, and lesion detectability compared to HS mode.

Keywords: Total-Body PET/CT Scanner; LAFOV PET/CT; low-dose [^{18}F]FDG PET; [^{18}F]FDG

1. Introduction

Positron emission tomography and computed tomography (PET/CT) hybrid imaging plays a fundamental role in current medical practice. Thereby, [^{18}F]fluoro-deoxy-glucose (FDG) PET/CT has become an essential pillar in the diagnosis and follow-up of various oncological diseases, such as lymphoma, melanoma, and lung cancer [1–3]. Recent advances in the field of PET/CT technology have led to the introduction of total-body (TB) PET/CT scanners with an extended axial field-of-view (aFOV), enabling the improvement of existing clinical applications and the establishment of new ones [4,5]. The extended aFOV of these scanners, ranging between 64 to 200 cm, increases solid angle coverage for the detection of coincident events, providing a higher sensitivity and relevant improvements in signal-to-noise ratio (SNR) compared to conventional PET scanners with shorter aFOVs [6,7]. Notably, the improved sensitivity is advantageous for examinations with low event

 doi:10.20944/preprints202310.0113.v1

statistics, such as PET imaging with radioisotopes with low branching ratios such as Y-90 [8,9], allowing for post-therapeutic PET scans after trans-arterial radioembolization with Y-90 microspheres; immuno-PET imaging with long half-life radioisotopes such as Zr-89 [10,11], which allows improved in vivo characterization of various tumors such as HER2-positive breast cancer [12]; and examinations with reduced doses of injected activity, contributing to a reduction in radiation exposure [13,14].

Conventional PET/CT scanners with a short aFOV of approximately 20 to 25 cm typically have a sensitivity in the range of 6 to 20 kcps/MBq [15]. In these scanners, roughly 85 to 90% of the body is located outside the aFOV, and only around 3 to 5% of the available signal within the FOV can be used [16]. In contrast, the Biograph Vision Quadra PET/CT scanner (Siemens Healthineers, Knoxville, TN, USA) provides an aFOV of 106 cm and a sensitivity of 83 kcps/MBq using its standard high-sensitivity (HS) mode with an acceptance angle of 18°. Compared to its predecessor model with a short aFOV (Biograph Vision 600) [17], the Biograph Vision Quadra features an approximately fivefold sensitivity increase [18].

The ultra-high sensitivity (UHS) mode, representing the latest sensitivity mode for the Biograph Vision Quadra, allows for the unlimited acceptance angle of 52°, further improving the sensitivity to 176 kcps/MBq. This improvement translates into an approximately two-fold increase in sensitivity compared to the standard HS mode [19]. This enables a further reduction of acquisition time while maintaining noise performance and might also provide advantages for low-dose examination protocols while maintaining diagnostic reliability. Despite these encouraging results, the standardization of short acquisition time and low-dose protocols in clinical routine remains to be achieved. Specifically, to the best of our knowledge, no studies have yet been published systematically evaluating the limits of reduction of injected activity regarding qualitative and quantitative image parameters in [^{18}F]FDG PET/CT of oncological patients on the Biograph Vision Quadra system.

Therefore, this study aimed to assess the impact of reduced [^{18}F]FDG activity doses on image quality and noise, lesion detectability, and uptake quantification while comparing the HS and UHS modes in the Siemens Biograph Vision Quadra PET/CT scanner.

2. Materials and Methods

Study Design and Patient Population

Twenty-six patients who underwent a whole-body [^{18}F]FDG PET/CT on a Biograph Vision Quadra PET/CT scanner were included in this retrospective analysis. PET/CT examinations were clinically indicated for oncological purposes. Patient characteristics are provided in **Supplementary Table 1**.

Imaging Protocol

Patients were required to fast for at least 10 hours prior to the examination. A venous blood glucose measurement was conducted to confirm blood glucose levels < 130 mg/dl. A standard dose of 3.0 MBq/kg [^{18}F]FDG was injected intravenously, and PET/CT image acquisition was started at 60 min. p.i.. Whole-body scans were acquired in a supine position covering an area from the head to the mid-thighs. Technical details of the CT image acquisition and protocol are provided in **Supplementary Table 2**. PET emission data with a routine acquisition time of 5 min. were acquired directly after the CT scan.

Image Reconstruction

PET image reconstruction was performed using the proprietary e7 tools software version VR20 (Siemens Healthineers, Knoxville, TN, USA). According to our standard clinical reconstruction protocol, an Ordinary-Poisson Ordered-Subsets Expectation-Maximization algorithm with four iterations and five subsets (OP-OSEM 4i5s) was applied, using point-spread-function (PSF) modeling and time-of-flight (TOF) information. PET images were reconstructed with a matrix of 440 x 440 x 645 with a 1.65 x 1.65 x 1.65 mm^3 isotropic voxel size, and no image filter was applied. Attenuation correction was performed based on the diagnostic CT scan acquired before the emission measurements. All reconstructions were performed for both the HS and the UHS mode. PET raw

 doi:10.20944/preprints202310.0113.v1

data (5 min. scan, 3.0 MBq/kg) was consecutively rebinned for shorter frame durations to simulate lower activities of injected [^{18}F]FDG as follows: 1.0 MBq/kg, 0.5 MBq/kg, 0.25 MBq/kg, and 0.125 MBq/kg. An example of a data set reconstructed with the different simulated doses and both sensitivity modes is shown in **Figure 1**.

Image Analysis and Evaluation

Image analysis and evaluation were performed on a dedicated workstation using the SyngoVia® software (Siemens Healthineers; Knoxville, TN, USA) by two experienced resident nuclear medicine physicians (one being a board-certified radiology physician, both with multi-year experience in the reading of oncological PET/CT scans) in consensus. Both readers were blinded to patient demographics and clinical information. Scans were read in multiple sessions in a randomized order. Afterward, all reconstructions per patient were re-read simultaneously to analyze lesion uptake. In patients with multifocal disease, a maximum of five lesions per patient were analyzed to reduce over-representation.

Subjective PET Image Quality

Subjective overall impression of image quality, subjective image noise, and conspicuity of suspected pathological lesions were assessed using a 5-point Likert scale. Criteria for the Likert scoring system are provided in **Table 1**.

Table 1: 5-Point Likert scoring system for subjective PET image rating.

Score	Image quality	Lesion conspicuity	Image noise
5	state-of-the-art quality	well-defined	near-imperceptible noise
4	superior to the average	fairly defined	lower than regular image of daily practice
3	regular quality of daily practice	hazy, recognizable	similar to regular image of daily practice
2	barely diagnostic	ill-defined, impairing diagnostic confidence	increased noise, slightly worse than regular image of daily practice
1	non-diagnostic	un-recognizable	excessive noise

Quantitative PET Analyses

Target lesion uptake was determined by placing a 40% isocontour volume of interest (VOI) around the lesion. Thereby, mean, peak, and maximum standardized uptake values (SUV_{mean}, SUV_{peak}, and SUV_{max}) were evaluated. As previously described, the liver was chosen to measure background activity [20]. Background uptake was determined by a 14 cm^3 VOI in healthy tissue of the right liver lobe. Target lesions were manually segmented in the standard scan (3.0 MBq/kg, 5 min., HS mode). Afterwards, corresponding VOIs were automatically overlayed onto the simulated scans, ensuring that the placement of the respective VOIs was identical in all data sets.

Preprints (www.preprints.org) | NOT PEER-REVIEWED | Posted: 4 October 2023 doi:10.20944/preprints202310.0113.v1

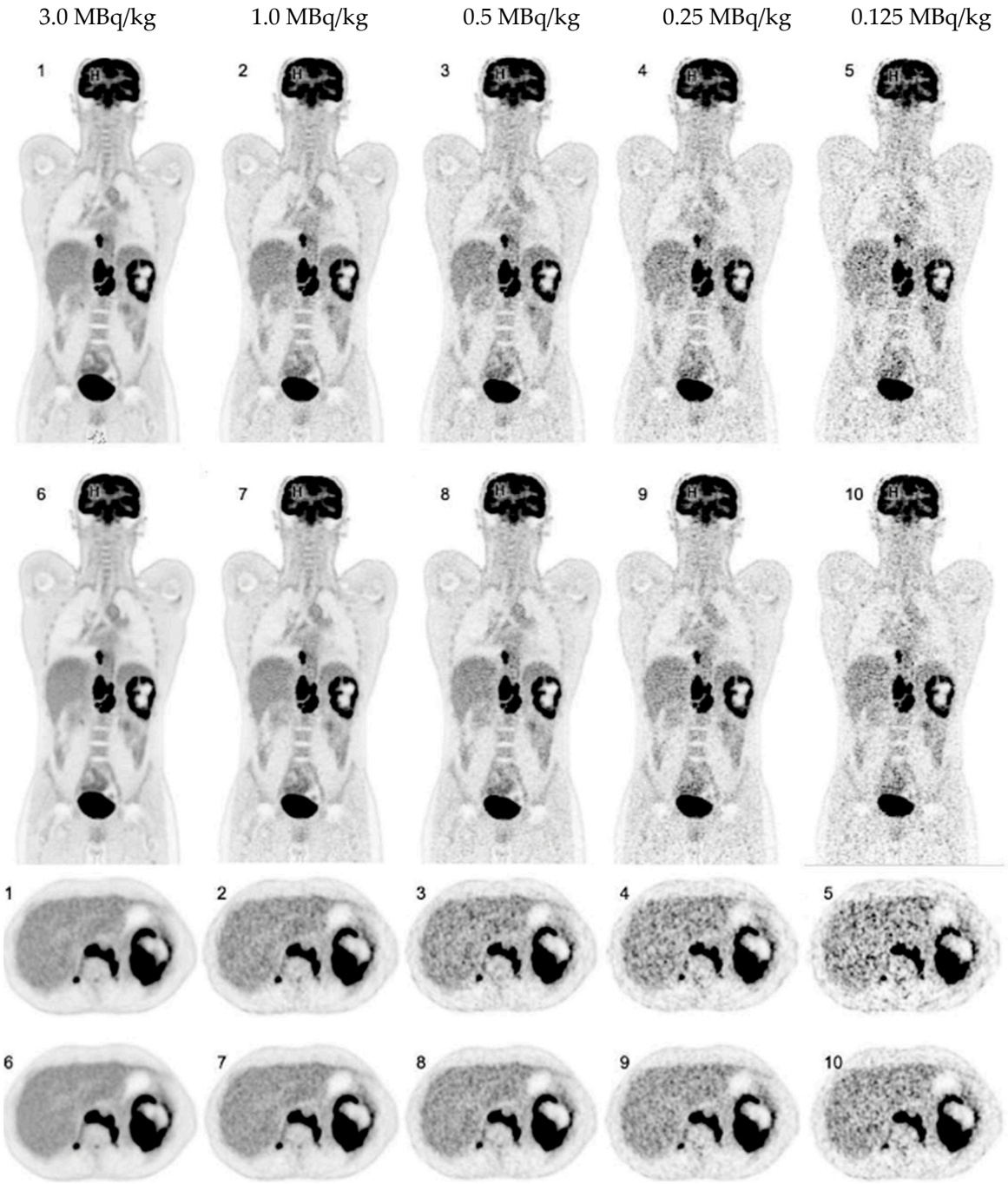

Figure 1: Coronal and axial [^{18}F]FDG PET images of a 37-year-old patient with Hodgkin lymphoma reconstructed in HS (1-5) and UHS (6-10) mode.

The tumor-to-background ratio (TBR) was calculated as an estimate for objective lesion contrast and lesion visibility as previously described [6]:

$$TBR = \frac{SUVpeakLesion}{SUVmeanBackground}$$

Furthermore, to quantitatively assess image noise, the coefficient of variation (CoV) was calculated using the following formula as previously published [21]:

$$CoV = \frac{SUVSD}{SUVmean}$$

A CoV of <15% (as a recommended threshold by the EFOMP and EANM [22]) was considered for interpretation. According to [19], the SNR was defined as the reciprocal variable of (CoV) for the

Preprints (www.preprints.org) | NOT PEER-REVIEWED | Posted: 4 October 2023 doi:10.20944/preprints202310.0113.v1

liver background. To account for physiological uptake differences between patients, the measured SUV from the different simulations was normalized to the corresponding SUV derived from the standard scan (3.0 MBq/kg, 5 min., HS mode). Subsequently, the normalized SUV mean values and standard deviations (SD) were determined.

Radiation Exposure

The effective radiation dose of the simulated examinations was calculated using the conversion factor of 0.019 mSv/MBq, as proposed by the International Commission on Radiological Protection publication 106 [23].

Statistical Analysis

Two-way ANOVA was performed to analyze the effect of simulated reduced dose and sensitivity modes on uptake values and SNR. Bonferroni´s multiple comparison tests were used to point out specific statistical significances following two-way ANOVA. Results of the two-way ANOVA are shown with p-values. An alpha level of 0.05 and a confidence interval of 95% were used for analysis. Corresponding degrees of freedom (df), F-values (F), and results of multiple comparison tests are provided in **Supplementary Tables 3 and 4**. Statistical analysis was performed using GraphPad Prism Version 9.4.1 (GraphPad Software, San Diego, California, USA).

3. Results

3.1. Overall PET Image Quality

The standard clinical scans with a dose of 3.0 MBq/kg in HS mode were subjectively rated with a mean Likert score of 4.0±0.4 (superior to the average quality). Reconstructed images with a dose reduction to 1.0, 0.5, 0.25 and 0.125 MBq/kg in HS mode were subsequently rated with mean Likert scores of 3.1±0.3, 2.0±0.3, 1.0±0.2 and 1.0±0.0 respectively.

Regarding image reconstructions in UHS mode compared to HS mode, subjective image quality was generally rated superior. At full doses of 3.0 MBq/kg in UHS mode, image quality was rated best, corresponding to "state-of-the-art quality" (Likert score 5.0±0.0). Reconstructed images with UHS mode received a rating of 4.1±0.3, 2.9±0.3, 1.9±0.3 and 1.1±0.3 for 1.0, 0.5, 0.25 and 0.125 MBq/kg, respectively. However, images at very low doses of 0.125 MBq/kg were not better rated as images in HS mode. Results of subjective quality ratings are provided in **Figure 2 (A)**.

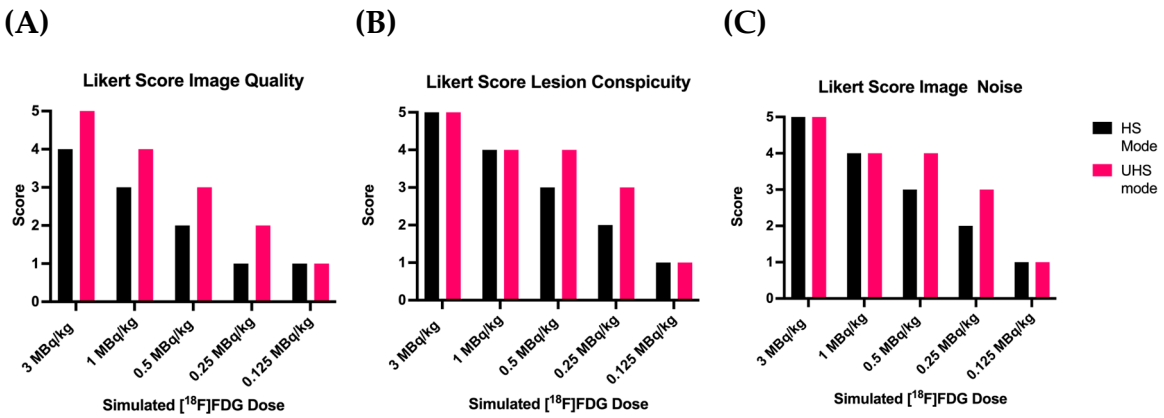

UHS: ultra-high sensitivity; HS: high sensitivity.

Figure 2: Results of subjective PET image quality ratings. **A**: Overall Image Quality; **B**: Lesion Conspicuity; and **C**: Image Noise.

3.2. Detectability and Conspicuity of Suspected Pathological Lesions

Results of lesion detectability are provided in **Table 2**. In total, 82 lesions were selected in the standard reference scan with 3.0 MBq/kg in HS mode and were considered for further analysis. Lesion detectability was not affected by sensitivity modes in dose reductions down to 1.0 MBq/kg.

Preprints (www.preprints.org) | NOT PEER-REVIEWED | Posted: 4 October 2023 doi:10.20944/preprints202310.0113.v1

The lesion detection rate decreased to 95%, 58%, and 40% (HS) and 98%, 68%, and 49% (UHS) for 0.5 MBq/kg, 0.25 MBq/kg and 0.125 MBq/kg, respectively.

Concerning subjective lesion conspicuity, all lesions were rated as "well-defined" at 1.0 MBq/kg with no notable different scoring between the HS and UHS mode (Likert score HS 3.8 ±0.4 and UHS 4.1±0.3). At 0.5 MBq/kg in HS mode, lesions were "hazy but recognizable" (Likert score 3.0±0.2). At 0.25 MBq/Kg in HS mode, lesions were considered "ill-defined, significantly impairing diagnostic confidence" (Likert score 2.0±0.5). PET image reconstructions in UHS mode at 0.5 MBq/Kg (Likert score 3.9±0.3) and 0.25 MBq/kg (Likert score HS 3.2±0.4) improved lesion conspicuity. However, at the lowest simulated dose of 0.125 MBq/kg, lesions were rated as mostly "unrecognizable" (Likert score HS 1.0±0.0 and UHS 1.1±0.3), independent of the sensitivity mode.

Table 2: Lesion detection rate according to simulated dose and sensitivity mode.

[^{18}F]FDG MBq/kg	Sensitivity mode	Number of lesions detected	Lesion detection rate in %
3.0	UHS	82	100%
3.0	HS	82	100%
1.0	UHS	82	100%
1.0	HS	82	100%
0.5	UHS	80	98%
0.5	HS	78	95%
0.25	UHS	68	83%
0.25	HS	58	71%
0.125	UHS	49	60%
0.125	HS	40	49%

UHS: ultra-high sensitivity; HS: high sensitivity.

Regarding lesion morphology in the CT scan, the mean size of every undetected lesion was 1.5 ± 0.57 cm and comprised almost exclusively small lymph nodes with a low to moderate [^{18}F]FDG uptake (SUV_{mean} 4.7±2.8). An example of a lesion being undetected in reconstructions with lower doses is provided in **Figure 3**.

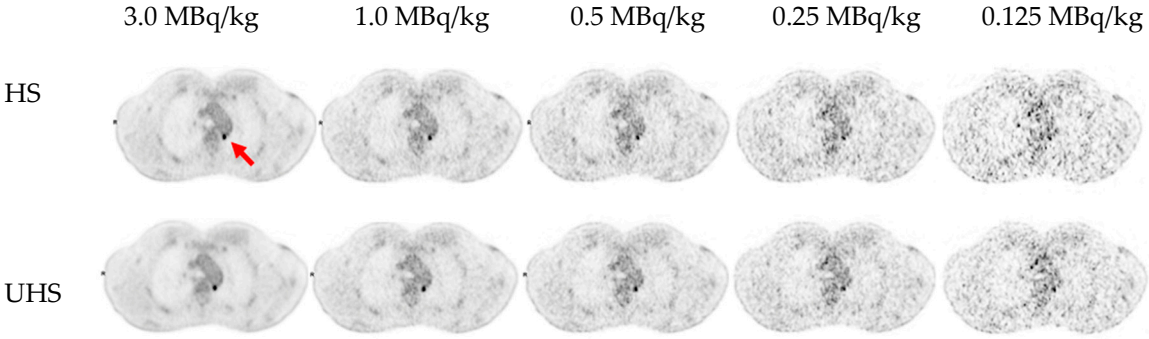

Figure 3: Example of a small retro-aortic lymph node (7 x 6 mm^2) undetected in reconstructions with lower doses (0.25 MBq/kg in HS mode and 0.125 MBq/kg in both HS and UHS mode).

3.3. Image Noise

Regarding subjective image noise ratings according to the Likert scale (**Figure 2(C)**), standard clinical images (3.0 MBq/kg, both in HS and UHS mode) were considered to show a "near imperceptible noise", corresponding to a Likert score of 5. Subjective image noise Likert scores of 4.8±0.4, 4.0±0.3, 3.0±0.3, 2.1±0.3 and 1.0±0.2 (HS) and 5.0±0.0, 4.3±0.5, 4.0±0.2, 3.2±0.4, and 1.2±0.4 (UHS) for 3.0, 1.0, 0.5, 0.25 and 0.125MBq/kg, respectively.

Detailed results of CoV and SNR measurements are provided in **Table 3 and Figure 4.** At 1.0 MBq/kg in HS mode, a mean CoV of 17.9±1.4% was recorded, slightly surpassing the recommended CoV <15.0% threshold. The mean CoV in HS mode for 0.5 MBq/kg, 0.25 MBq/kg, and 0.125 MBq/Kg were 25.3±1.9%, 35.5±4.0%, and 49.0±6.3%, respectively. For the UHS mode, the CoV was always

Preprints (www.preprints.org) | NOT PEER-REVIEWED | Posted: 4 October 2023 doi:10.20944/preprints202310.0113.v1

lower; therefore, the same image noise could be obtained for UHS as for HS for lower doses, e.g., a CoV of 18.3%±1.8% (0.5 MBq/kg, UHS), which is comparable to 17,9±2,0% with 1.0 MBq/kg in HS mode.

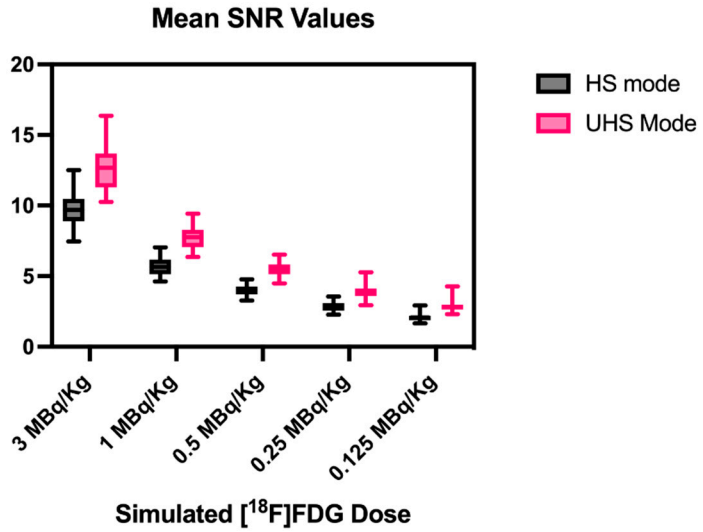

HS: high sensitivity; UHS: ultra-high sensitivity; SNR: signal-to-noise ratio.

Figure 4. Mean SNR values of liver background according to simulated dose and sensitivity mode.

Two-way ANOVA on SNR values revealed a statistically significant interaction between the effects of the sensitivity mode and simulated dose reduction ($p<0.0001$). Furthermore, the results of the main effects showed that, in general, the sensitivity mode and simulated dose reduction have independently a statistically significant effect on SNR values ($p<0.0001$ for each main effect). The Post-hoc multiple comparison test revealed that the mean values of SNR were significantly different between almost every simulated dose and sensitivity mode. This was, however, not the case between reconstructions in HS mode and reconstructions in UHS mode with half the simulated dose (e.g., 1.0 MBq/kg HS mode vs. 0.5 MBq/kg UHS mode, $p>0.99$). Furthermore, a mean SNR UHS/HS ratio of all reconstructed images of 1.36 ± 0.02 was reported.

Table 3: Coefficient of Variation and signal-to-noise ratio according to simulated dose and sensitivity mode.

[18F]FDG MBq/kg	Sensitivity mode	Mean CoV and STD in %	Mean SNR and STD
3.0	UHS	7.9±0.9	12.8±1.6
3.0	HS	10.4±1.2	9.7±1.1
1.0	UHS	13.0±1.3	7.8±0.8
1.0	HS	17.8±1.9	5.7±0.6
0.5	UHS	18.3±1.7	5.5±0.5
0.5	HS	25.2±2.5	4.0±0.4
0.25	UHS	26.0±3.3	3.9±0.5
0.25	HS	35.5±4.0	2.9±0.3
0.125	UHS	35.5±4.7	2.9±0.5
0.125	HS	48.9±6.3	2.1±0.3

UHS: ultra-high sensitivity; HS: high sensitivity; CoV: coefficient of variation; STD: standard deviation; SNR: signal-to-noise ratio.

Preprints (www.preprints.org) | NOT PEER-REVIEWED | Posted: 4 October 2023 doi:10.20944/preprints202310.0113.v1

3.4. Quantitative PET Parameters

Graphics displaying the results of quantitative PET parameters are provided in **Figure 5**. Both SUV_{mean} and SUV_{peak} only showed minimal decreases in simulated low-dose reconstructions. Regarding the lowest dose of 0.125 MBq/kg, SUV_{mean} decreased by only 8%, whereas SUV_{peak} decreased by only 3%. The impact of the sensitivity mode on SUV_{mean} and SUV_{peak} values was negligible. Two-way ANOVA revealed no statistically significant interaction between the effects of sensitivity mode and reduced doses, neither for SUV_{mean} nor SUV_{peak} ($p>0.99$). Main effects analysis showed that neither sensitivity mode nor simulated dose reduction alone had a statistically significant effect on SUV_{mean} or SUV_{peak} values ($p=0.76$, $p=0.76$, $p=0.93$, $p=0.81$, respectively).

SUV_{max} increased steadily for lower doses (**Figure 5(C)**): However, the increase was less prominent for UHS in comparison to HS mode, e.g., we reported an increase of 16% (HS) and 6% (UHS) at 0.5 MBq/kg and 27% (HS) and 13% (UHS) at 0.25 MBq/kg. Two-way ANOVA showed no statistically significant interaction between the effects of the sensitivity mode and simulated dose reduction ($p=0.92$) on SUV_{max}. Consistently, post-hoc multiple comparison tests revealed that the significant difference in SUV_{max} values was present only when comparing values between the standard scan (3.0 MBq/kg, HS mode) with 0.125 MBq/kg in HS mode ($p=0.0135$), where a mean increase of 41% was recorded. Main effects analysis shows that both simulated dose reduction and sensitivity mode had a statistically significant effect on SUV_{max} values ($p=0.003$, $p=0.04$).

Regarding TBR (as a function of SUV_{peak}), two-way ANOVA revealed no statistically significant interaction between the effects of simulated dose reduction and sensitivity mode ($p>0.99$, $p=0.88$). Moreover, the main effects analysis showed that neither simulated dose reduction nor sensitivity mode had a statistically significant effect on TBR values.

Preprints (www.preprints.org) | NOT PEER-REVIEWED | Posted: 4 October 2023 doi:10.20944/preprints202310.0113.v1

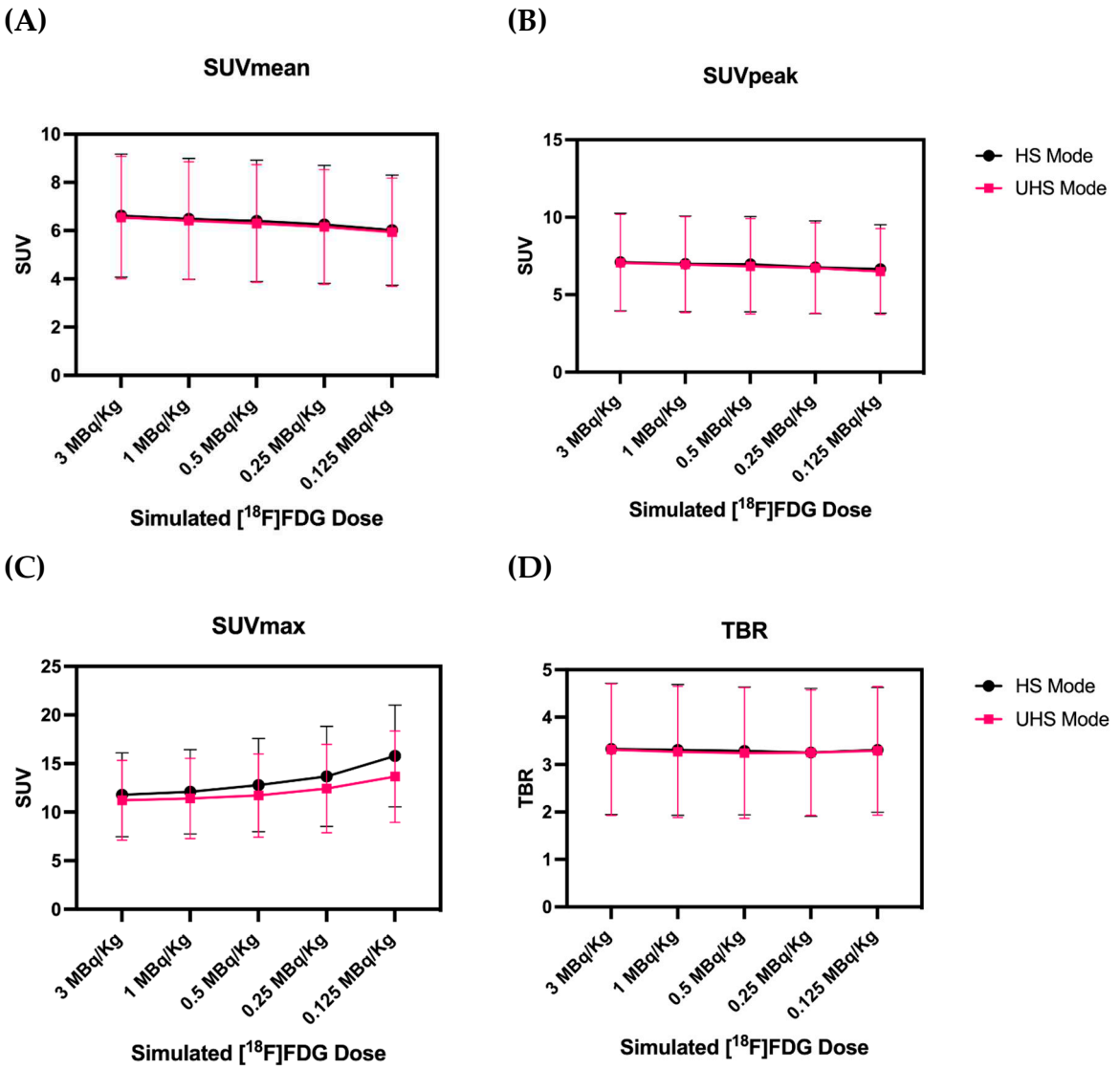

UHS: ultra-high sensitivity: HS, high sensitivity; STD: standard deviation; AU: arbitrary unit.

Figure 5: Average values of all lesions for SUV_{mean} **(A)**, SUV_{peak} **(B)**, SUV_{max} **(C)**, and TBR **(D)** for different simulated doses.

4. Discussion

Recent studies have demonstrated the improved performance characteristics of total-body PET/CT scanners. For example, studies evaluating the uEXPLORER, another commercially available TB PET/CT scanner with an aFOV of approximately 2 meters, showed that low- (1.85 MBq/kg) or ultra-low-dose (0.37 MBq/kg) imaging protocols [24,25] may be clinically feasible, usually requiring longer scan times (>5 min.).

For the Biograph Vision Quadra, a study in melanoma patients showed that a dose reduction down to 2.0 MBq/Kg with a 5 min. scan was not associated with worsening clinical performance [13]. Such protocols may profit from the recently introduced UHS mode, which has the potential to further lower both acquisition time and/or applicated activity by fully exploiting the largely increased sensitivity of this total-body PET/CT scanner. However, before low-dose protocols involving this new sensitivity mode can be implemented into routine clinical practice, evaluating their limitations and diagnostical reliability is necessary. Therefore, we assessed the influence of reduced [18F]FDG activity

 doi:10.20944/preprints202310.0113.v1

doses for both HS and UHS modes on qualitative and quantitative PET parameters in the Biograph Vision Quadra.

Regarding subjective image rating, we determined that images at 0.5 MBq/kg (1/6th of the standard clinical dose) with 5 min. acquisition in HS mode were "barely diagnostic". In this regard, simulations with very low doses in HS mode (0.25 MBq/kg and 0.125 MBq/kg) were rated as biased by the poor image quality and affected diagnostic reliability. However, using the same protocols in UHS mode, improved diagnostic image quality was consistently achieved, e.g. images at 0.25 MBq/kg in UHS mode were then also rated as "barely diagnostic". We would still however recommend that these very low doses should not be considered for clinical application unless compensated by a scan time considerably longer than 5 min. In general, the enhanced SNR in UHS mode led to an overall improvement in the subjectively evaluated image characteristics, except for 0.125 MBq/kg, where no tangible improvements were noted.

Lesion detectability decreased at the dose of 0.5 MBq/kg to a detection rate of 95% in HS mode and could be partly recovered to 98% in UHS mode. Lesion morphology and tracer uptake evidently influenced lesion detection. The mean size of undetected lesions was 1.5 ± 0.57 cm with a SUV_{mean} of 4.7 ± 2.8, mainly indicating an increased risk of smaller and low to moderate metabolic active lesions remaining undetected.

A dose of 1.0 MBq/kg combined with the HS mode resulted in a CoV of 17.9% ± 2.0, exceeding the threshold of 15.0% recommended by EFOMP and EANM [22]. The UHS mode could meet this criterion with a CoV of 13.0±1.3%. To further reduce the dose and maintain an acceptable image noise, filtering of the images can be performed. In this regard, Rausch et al. [26] showed that for the Biograph Vision Quadra, using a 6 mm Gaussian filter instead of a 2 mm filter helped to increase the useful aFOV (CoV < 15%) from 83 cm to 103 cm. Subjective image noise ratings considered noise excessive and impairing diagnostic quality at less than 0.25 MBq/Kg while having acceptable image noise levels even at 0.5 MBq/kg, implying that higher noise values may still be acceptable in clinical settings.

Furthermore, two-way ANOVA showed that the SNR values of images reconstructed in UHS mode have comparable SNRs to images reconstructed in HS mode but with twice the simulated activity, e.g 0.5 MBq/kg (UHS) vs 1.0 MBq/kg (HS), which is another way of interpreting similar results previously published, where 30 s/60 s acquisitions in UHS showed comparable SNRs to 60 s/120 s acquisitions in HS mode [19]. Furthermore, a mean SNR UHS to HS ratio of 1.36 ± 0.02 was reported, which also aligns with previously published values. The UHS mode is, thus, useful for acquiring clinically diagnostic images with lower activity protocols.

Of note, image noise is not uniformly improved across the FOV. Schmidt et al. [27] reported that for the Biograph Vision Quadra, the improvement in CoV in the center FOV can be as high as a factor of 1.49, comparing UHS and HS mode. However, no improvement was observed with the UHS mode beyond the central 80 cm of the aFOV.

Concerning quantitative PET parameters, SUV_{mean}, SUV_{peak}, and TBR showed only minimal decreases of <10% and two-way ANOVA revealed no statistically significant differences, including at the lowest simulated dose. $SUV_{max,}$ however, was considerably higher for the HS mode and increased towards lower doses, which is comparable to previously published results, where 600s acquisitions had statistically significant differences in SUV_{max} values of evaluated lesions compared to 120s and 60s acquisitions [28], whereas SUV_{mean} and SUV_{peak} remained relative stable. This is expected to be caused by the influence of noise on SUV_{max} [29,30]. In our study, two-way ANOVA and multiple comparisons revealed only statistically significantly differences while comparing SUV_{max} values between the standard 3.0 MBq/kg scan in HS mode at 0.125 MBq/kg in HS mode, with values not being statistically significantly different compared with 0.125 MBq/kg in UHS mode.

SUV_{max} is known to be overestimated due to the PSF reconstruction [31,32] and prone to noise distortion as it is based on the value of only a single voxel. Therefore, using SUV_{peak} or SUV_{mean} for quantification instead of SUV_{max} seems reasonable, especially in scenarios with low event statistics. The fact that the uptake values remained relatively constant at lower doses down to 0.125 MBq/kg

 doi:10.20944/preprints202310.0113.v1

(=1/24th of the standard applied dose, UHS mode) indicates that the fundamental limitations regarding dose reduction were based on insufficient diagnostic image quality.

Considering the results of this study, the Biograph Vision Quadra and total-body PET/CT scanners, in general, provide an emerging flexibility regarding applied activities. Of note, instead of altering the dose, a change in scan duration can also have a comparable impact. As such, considering the short half-life of F-18 of 109.8 min, a 5 min. scan with 1.0 MBq/kg would yield approximately the same count statistics as a 10 min. scan with 0.5 MBq/kg. As with 1.0 MBq/kg, no degradations were reported in our work compared to the full 3.0 MBq/kg with a 5 min. scan. This implies the same is true for 0.5 MBq/kg with a 10 min scan time. This would allow high image quality, quantification accuracy, and diagnostic reliability with an effective dose of less than 1 mSv (for a 70kg patient).

Utilizing this protocol with 0.5 MBq/kg and a 10-minute scan would also allow feasible dual-tracer same-day protocols, for example, by performing an [^{18}F]FDG PET early in the day. Approximately three half-lives later, one could perform a second PET scan with a different radiotracer and standard activity doses (2.0-3.0 MBq/kg) of e.g. [^{18}F]PSMA-1007 or [^{18}F]SiFAlin-TATE, since no relevant activity remains at the time of the second scan. Such protocols would come into question where the [^{18}F]FDG PET supports clinical decision-making, for example, for patient selection or therapy control in patients with prostate cancer or neuroendocrine tumors that may receive or are receiving radioligand therapy. This type of examination aims to find radiotracer mismatches (FDG-positive and PSMA/SSR negative), which may indicate more aggressive tumor types that may warrant more aggressive therapy regimens instead of radioligand therapy [33]. The benefit of this protocols compared to previously published ones, e.g., first completion of [^{68}Ga]Ga-PSMA-11 PET scan followed immediately by a standard 40 MBq injection of [^{18}F]FDG [34], is that the semi-quantitative assessment of both FDG and PSMA would be less problematic at the cost of longer waiting times for patients. Nonetheless, both protocols would be able to assess radiotracer mismatches.

Considering the reduced radiation exposure, pediatric patients could also benefit, and hybrid imaging could become more feasible in this patient population. The flexibility of total-body PET/CT scanners comes to note in pediatric patients since, depending on the clinical setting, one would be able to apply a standard activity dose and perform a fast scan while avoiding the use of anesthesia, as Reichkendler M et al. showed [35], or reduce applied activity in children that don't require sedation. Our results might be transferable for hybrid imaging studies in the pediatric population, but this requires further evaluation.

One limitation of this study is that only a relatively small sample size of 26 patients with a total of 82 pathological target lesions was included for analysis. Only two patients included were obese with a BMI > 35 kg/m^2. Previous studies reported that a dose reduction was feasible only in non-obese patients with a BMI < 30 kg/m2, thus limiting the generalizability of our results to the obese patient population [36]. Another limitation is that only [^{18}F]FDG in oncological patients was considered in this study, and no non-oncological indications for PET/CT (e.g., search for florid inflammation or fever of unknown origin) were analyzed. Furthermore, the transferability to tracers based on isotopes different than F-18, which have a larger positron range (such as Ga-68) or typically require lower activities (such as Zr-89), need to be elaborated as these impact quantification accuracy and noise performance [37]. Further studies are warranted to assess the feasibility of low-dose PET examinations in these scenarios.

5. Conclusions

Due to their high sensitivity, total-body PET/CT scanners allow for a considerable reduction of applied activity of radiotracers. In this study, we showed that reducing injected [^{18}F]-FDG activity to 1.0 MBq/kg in a TB PET/CT still offered clinically diagnostic image quality without relevant changes in uptake parameters. Further reductions appear feasible by prolonging scan times (e.g., 10 minutes) and by using UHS mode. Fundamental limitations of further dose reduction were based on insufficient diagnostic image quality and diminishing performance, and not involving possible alterations of quantitative uptake parameters. These novel insights may further expand the

implementation in clinical routine, possibly allowing for e.g., same-day multi-tracer protocols and applications in pediatric patient populations.

Supplementary Materials: The following supporting information can be downloaded at the website of this paper posted on Preprints.org.

Author Contributions: Conceptualization, Eduardo Calderón , Fabian Schmidt, Christian la Fougère and Lena Kiefer; Data curation, Eduardo Calderón , Fabian Schmidt, Wenhong Lan and Salvador Castaneda-Vega; Formal analysis, Eduardo Calderón , Fabian Schmidt, Salvador Castaneda-Vega, Nils Trautwein and Lena Kiefer; Funding acquisition, Christian la Fougère and Lena Kiefer; Investigation, Eduardo Calderón , Fabian Schmidt and Lena Kiefer; Methodology, Eduardo Calderón , Fabian Schmidt, Wenhong Lan and Lena Kiefer; Project administration, Eduardo Calderón , Fabian Schmidt, Helmut Dittmann and Christian la Fougère; Resources, Fabian Schmidt, Andreas Brendlin and Christian la Fougère; Software, Eduardo Calderón , Fabian Schmidt, Wenhong Lan and Salvador Castaneda-Vega; Supervision, Fabian Schmidt, Helmut Dittmann, Christian la Fougère and Lena Kiefer; Validation, Eduardo Calderón , Fabian Schmidt, Helmut Dittmann and Lena Kiefer; Visualization, Eduardo Calderón and Lena Kiefer; Writing – original draft, Eduardo Calderón and Lena Kiefer; Writing – review & editing, Eduardo Calderón , Fabian Schmidt, Wenhong Lan, Salvador Castaneda-Vega, Nils Trautwein, Helmut Dittmann, Christian la Fougère and Lena Kiefer.

Funding: The Total-Body PET/CT scanner was funded by the Deutsche Forschungsgemeinschaft (DFG, German Research Foundation) – INST 37/1145-1 FUGG. Funded by the Deutsche Forschungsgemeinschaft (DFG, German Research Foundation) under Germany's Excellence Strategy - EXC 2180 – 390900677. Lena Sophie Kiefer received a grant from the Faculty of Medicine, Tuebingen, Germany (TÜFF, No. 2727-0-0).

Institutional Review Board Statement: The study was conducted according to the guidelines of the Declaration of Helsinki and approved by the Institutional Review Board of the University Hospital of Tuebingen (#167/2020BO2).

Informed Consent Statement: Patient consent was waived due to retrospective data acquisition.

Acknowledgments: The Total-Body PET/CT scanner was funded by the Deutsche Forschungsgeminschaft (DFG, German Research Foundation) – INST 37/1145-1 FUGG.

Conflicts of Interest: Schmidt F. and la Fougère C. received a research grant from Siemens Healthineers. No other potential conflicts of interest relevant to this article exist. The funders had no role in the design of the study; in the collection, analyses, or interpretation of data; in the writing of the manuscript; or in the decision to publish the results.

References

1. Farsad, M. FDG PET/CT in the Staging of Lung Cancer. Curr Radiopharm 2020, 13, 195–203, doi:10.2174/1874471013666191223153755.
2. Ayati, N.; Sadeghi, R.; Kiamanesh, Z.; Lee, S.T.; Zakavi, S.R.; Scott, A.M. The Value of 18F-FDG PET/CT for Predicting or Monitoring Immunotherapy Response in Patients with Metastatic Melanoma: A Systematic Review and Meta-Analysis. Eur J Nucl Med Mol Imaging 2021, 48, 428–448, doi:10.1007/s00259-020-04967-9.
3. Zanoni, L.; Bezzi, D.; Nanni, C.; Paccagnella, A.; Farina, A.; Broccoli, A.; Casadei, B.; Zinzani, P.L.; Fanti, S. PET/CT in Non-Hodgkin Lymphoma: An Update. Semin Nucl Med 2023, 53, 320–351, doi:10.1053/j.semnuclmed.2022.11.001.
4. Nadig, V.; Herrmann, K.; Mottaghy, F.M.; Schulz, V. Hybrid Total-Body Pet Scanners—Current Status and Future Perspectives. Eur J Nucl Med Mol Imaging 2022, 49, 445–459, doi:10.1007/s00259-021-05536-4.
5. Alavi, A.; Saboury, B.; Nardo, L.; Zhang, V.; Wang, M.; Li, H.; Raynor, W.Y.; Werner, T.J.; Høilund-Carlsen, P.F.; Revheim, M.-E. Potential and Most Relevant Applications of Total Body PET/CT Imaging. Clin Nucl Med 2022, 47, 43–55, doi:10.1097/RLU.0000000000003962.
6. Alberts, I.; Hünermund, J.-N.; Prenosil, G.; Mingels, C.; Bohn, K.P.; Viscione, M.; Sari, H.; Vollnberg, B.; Shi, K.; Afshar-Oromieh, A.; et al. Clinical Performance of Long Axial Field of View PET/CT: A Head-to-Head Intra-Individual Comparison of the Biograph Vision Quadra with the Biograph Vision PET/CT. Eur J Nucl Med Mol Imaging 2021, 48, 2395–2404, doi:10.1007/s00259-021-05282-7.
7. Dimitrakopoulou-Strauss, A.; Pan, L.; Sachpekidis, C. Long Axial Field of View (LAFOV) PET-CT: Implementation in Static and Dynamic Oncological Studies. Eur J Nucl Med Mol Imaging 2023, doi:10.1007/s00259-023-06222-3.
8. Attarwala, A.A.; Molina-Duran, F.; Büsing, K.-A.; Schönberg, S.O.; Bailey, D.L.; Willowson, K.; Glatting, G. Quantitative and Qualitative Assessment of Yttrium-90 PET/CT Imaging. PLOS ONE 2014, 9, e110401, doi:10.1371/journal.pone.0110401.

9. Dryák, P.; Šolc, J. Measurement of the Branching Ratio Related to the Internal Pair Production of Y-90. Applied Radiation and Isotopes 2020, 156, 108942, doi:10.1016/j.apradiso.2019.108942.
10. van Sluis, J.; Borra, R.; Tsoumpas, C.; van Snick, J.H.; Roya, M.; Ten Hove, D.; Brouwers, A.H.; Lammertsma, A.A.; Noordzij, W.; Dierckx, R.A.J.O.; et al. Extending the Clinical Capabilities of Short- and Long-Lived Positron-Emitting Radionuclides through High Sensitivity PET/CT. Cancer Imaging 2022, 22, 69, doi:10.1186/s40644-022-00507-w.
11. Mohr, P.; Sluis, J. van; Providência, L.; Snick, J.H. van; Hooge, M.N.L.; Willemsen, A.T.; Glaudemans, A.W.J.M.; Boellaard, R.; Lammertsma, A.A.; Brouwers, A.H.; et al. Long Versus Short Axial Field of View Immuno-PET/CT: Semiquantitative Evaluation for 89Zr-Trastuzumab. Journal of Nuclear Medicine 2023, doi:10.2967/jnumed.123.265621.
12. Lugat, A.; Bailly, C.; Chérel, M.; Rousseau, C.; Kraeber-Bodéré, F.; Bodet-Milin, C.; Bourgeois, M. Immuno-PET: Design Options and Clinical Proof-of-Concept. Front Med (Lausanne) 2022, 9, 1026083, doi:10.3389/fmed.2022.1026083.
13. Tan, H.; Sui, X.; Yin, H.; Yu, H.; Gu, Y.; Chen, S.; Hu, P.; Mao, W.; Shi, H. Total-Body PET/CT Using Half-Dose FDG and Compared with Conventional PET/CT Using Full-Dose FDG in Lung Cancer. Eur J Nucl Med Mol Imaging 2021, 48, 1966–1975, doi:10.1007/s00259-020-05091-4.
14. Sachpekidis, C.; Pan, L.; Kopp-Schneider, A.; Weru, V.; Hassel, J.C.; Dimitrakopoulou-Strauss, A. Application of the Long Axial Field-of-View PET/CT with Low-Dose [18F]FDG in Melanoma. Eur J Nucl Med Mol Imaging 2023, 50, 1158–1167, doi:10.1007/s00259-022-06070-7.
15. Surti, S.; Pantel, A.R.; Karp, J.S. Total Body PET: Why, How, What For? IEEE Trans Radiat Plasma Med Sci 2020, 4, 283–292, doi:10.1109/trpms.2020.2985403.
16. Cherry, S.R.; Jones, T.; Karp, J.S.; Qi, J.; Moses, W.W.; Badawi, R.D. Total-Body PET: Maximizing Sensitivity to Create New Opportunities for Clinical Research and Patient Care. J Nucl Med 2018, 59, 3–12, doi:10.2967/jnumed.116.184028.
17. Prenosil, G.A.; Sari, H.; Fürstner, M.; Afshar-Oromieh, A.; Shi, K.; Rominger, A.; Hentschel, M. Performance Characteristics of the Biograph Vision Quadra PET/CT System with a Long Axial Field of View Using the NEMA NU 2-2018 Standard. J Nucl Med 2022, 63, 476–484, doi:10.2967/jnumed.121.261972.
18. Prenosil, G.A.; Hentschel, M.; Weitzel, T.; Sari, H.; Shi, K.; Afshar-Oromieh, A.; Rominger, A. EARL Compliance Measurements on the Biograph Vision Quadra PET/CT System with a Long Axial Field of View. EJNMMI Phys 2022, 9, 26, doi:10.1186/s40658-022-00455-1.
19. Mingels, C.; Weidner, S.; Sari, H.; Buesser, D.; Zeimpekis, K.; Shi, K.; Alberts, I.; Rominger, A. Impact of the New Ultra-High Sensitivity Mode in a Long Axial Field-of-View PET/CT. Ann Nucl Med 2023, 37, 310–315, doi:10.1007/s12149-023-01827-y.
20. Boellaard, R.; Delgado-Bolton, R.; Oyen, W.J.G.; Giammarile, F.; Tatsch, K.; Eschner, W.; Verzijlbergen, F.J.; Barrington, S.F.; Pike, L.C.; Weber, W.A.; et al. FDG PET/CT: EANM Procedure Guidelines for Tumour Imaging: Version 2.0. Eur J Nucl Med Mol Imaging 2015, 42, 328–354, doi:10.1007/s00259-014-2961-x.
21. De Luca, G.M.R.; Habraken, J.B.A. Method to Determine the Statistical Technical Variability of SUV Metrics. EJNMMI Physics 2022, 9, 40, doi:10.1186/s40658-022-00470-2.
22. EFOMP Protocol for Quality Control in PET/CT and PET/MRI Available online: https://www.efomp.org/index.php?r=news/view&id=277 (accessed on 22 May 2023).
23. Mattsson, S.; Johansson, L.; Leide Svegborn, S.; Liniecki, J.; Noßke, D.; Riklund, K.Å.; Stabin, M.; Taylor, D.; Bolch, W.; Carlsson, S.; et al. Radiation Dose to Patients from Radiopharmaceuticals: A Compendium of Current Information Related to Frequently Used Substances. Ann ICRP 2015, 44, 7–321, doi:10.1177/0146645314558019.
24. He, Y.; Gu, Y.; Yu, H.; Wu, B.; Wang, S.; Tan, H.; Cao, Y.; Chen, S.; Sui, X.; Zhang, Y.; et al. Optimizing Acquisition Times for Total-Body Positron Emission Tomography/Computed Tomography with Half-Dose 18F-Fluorodeoxyglucose in Oncology Patients. EJNMMI Phys 2022, 9, 45, doi:10.1186/s40658-022-00474-y.
25. Tan, H.; Cai, D.; Sui, X.; Qi, C.; Mao, W.; Zhang, Y.; Liu, G.; Yu, H.; Chen, S.; Hu, P.; et al. Investigating Ultra-Low-Dose Total-Body [18F]-FDG PET/CT in Colorectal Cancer: Initial Experience. Eur J Nucl Med Mol Imaging 2022, 49, 1002–1011, doi:10.1007/s00259-021-05537-3.
26. Rausch, I.; Mannheim, J.G.; Kupferschläger, J.; la Fougère, C.; Schmidt, F.P. Image Quality Assessment along the One Metre Axial Field-of-View of the Total-Body Biograph Vision Quadra PET/CT System for 18F-FDG. EJNMMI Phys 2022, 9, 87, doi:10.1186/s40658-022-00516-5.
27. Schmidt, F.; Rausch, I.; Mannheim, J.; Linder, P.; Will, P.; Conti, M.; Fougère, C. Impact of the Maximum Ring Difference on Image Quality and Noise Characteristics of a Total Body PET/CT Scanner.; March 30 2023; Vol. 62.
28. van Sluis, J.; van Snick, J.H.; Brouwers, A.H.; Noordzij, W.; Dierckx, R.A.J.O.; Borra, R.J.H.; Slart, R.H.J.A.; Lammertsma, A.A.; Glaudemans, A.W.J.M.; Boellaard, R.; et al. EARL Compliance and Imaging Optimisation on the Biograph Vision Quadra PET/CT Using Phantom and Clinical Data. Eur J Nucl Med Mol Imaging 2022, 49, 4652–4660, doi:10.1007/s00259-022-05919-1.

29. Koopman, D.; van Osch, J.A.C.; Jager, P.L.; Tenbergen, C.J.A.; Knollema, S.; Slump, C.H.; van Dalen, J.A. Technical Note: How to Determine the FDG Activity for Tumour PET Imaging That Satisfies European Guidelines. EJNMMI Physics 2016, 3, 22, doi:10.1186/s40658-016-0158-z.
30. Lodge, M.A.; Chaudhry, M.A.; Wahl, R.L. Noise Considerations for PET Quantification Using Maximum and Peak Standardized Uptake Value. J Nucl Med 2012, 53, 1041–1047, doi:10.2967/jnumed.111.101733.
31. Tsai, Y.-J.; Liu, C. Pitfalls on PET/CT Due to Artifacts and Instrumentation. Semin Nucl Med 2021, 51, 646–656, doi:10.1053/j.semnuclmed.2021.06.015.
32. Alessio, A.M.; Stearns, C.W.; Tong, S.; Ross, S.G.; Kohlmyer, S.; Ganin, A.; Kinahan, P.E. Application and Evaluation of a Measured Spatially Variant System Model for PET Image Reconstruction. IEEE Trans Med Imaging 2010, 29, 938–949, doi:10.1109/TMI.2010.2040188.
33. Buteau, J.P.; Martin, A.J.; Emmett, L.; Iravani, A.; Sandhu, S.; Joshua, A.M.; Francis, R.J.; Zhang, A.Y.; Scott, A.M.; Lee, S.-T.; et al. PSMA and FDG-PET as Predictive and Prognostic Biomarkers in Patients given [177Lu]Lu-PSMA-617 versus Cabazitaxel for Metastatic Castration-Resistant Prostate Cancer (TheraP): A Biomarker Analysis from a Randomised, Open-Label, Phase 2 Trial. The Lancet Oncology 2022, 23, 1389–1397, doi:10.1016/S1470-2045(22)00605-2.
34. Alberts, I.; Schepers, R.; Zeimpekis, K.; Sari, H.; Rominger, A.; Afshar-Oromieh, A. Combined [68 Ga]Ga-PSMA-11 and Low-Dose 2-[18F]FDG PET/CT Using a Long-Axial Field of View Scanner for Patients Referred for [177Lu]-PSMA-Radioligand Therapy. Eur J Nucl Med Mol Imaging 2023, 50, 951–956, doi:10.1007/s00259-022-05961-z.
35. Reichkendler, M.; Andersen, F.L.; Borgwardt, L.; Nygaard, U.; Albrecht-Beste, E.; Andersen, K.F.; Ljunggren, A.; Abrahamsen, N.; Loft, A.; Højgaard, L.; et al. A Long Axial Field of View Enables PET/CT in Toddler Without Sedation. Journal of Nuclear Medicine 2022, 63, 1962–1962, doi:10.2967/jnumed.121.263626.
36. Sekine, T.; Delso, G.; Zeimpekis, K.G.; de Galiza Barbosa, F.; Ter Voert, E.E.G.W.; Huellner, M.; Veit-Haibach, P. Reduction of 18F-FDG Dose in Clinical PET/MR Imaging by Using Silicon Photomultiplier Detectors. Radiology 2018, 286, 249–259, doi:10.1148/radiol.2017162305.
37. Mannheim, J.G.; Rausch, I.; Conti, M.; la Fougère, C.; Schmidt, F.P. Characterization of the Partial Volume Effect along the Axial Field-of-View of the Biograph Vision Quadra Total-Body PET/CT System for Multiple Isotopes. EJNMMI Physics 2023, 10, 33, doi:10.1186/s40658-023-00554-7.